

Organoruthenium(II) compounds with pyridyl benzoxazole/benzthiazole moiety: Studies on DNA/protein binding and enzyme mimetic activities

Asaithambi Gomathi, Paranthaman Vijayan, Periasamy Viswanathamurthi, Shanmugam Suresh, Raju Nandhakumar & Takeshi Hashimoto

To cite this article: Asaithambi Gomathi, Paranthaman Vijayan, Periasamy Viswanathamurthi, Shanmugam Suresh, Raju Nandhakumar & Takeshi Hashimoto (2017): Organoruthenium(II) compounds with pyridyl benzoxazole/benzthiazole moiety: Studies on DNA/protein binding and enzyme mimetic activities, Journal of Coordination Chemistry, DOI: [10.1080/00958972.2017.1309649](https://doi.org/10.1080/00958972.2017.1309649)

To link to this article: <http://dx.doi.org/10.1080/00958972.2017.1309649>

 View supplementary material 

 Accepted author version posted online: 20 Mar 2017.

 Submit your article to this journal 

 View related articles 

 View Crossmark data 

Publisher: Taylor & Francis

Journal: *Journal of Coordination Chemistry*

DOI: <http://dx.doi.org/10.1080/00958972.2017.1309649>

Organoruthenium(II) compounds with pyridyl benzoxazole/benzthiazole moiety: Studies on DNA/protein binding and enzyme mimetic activities

ASAITHAMBI GOMATHI[†], PARANTHAMAN VIJAYAN[†], PERIASAMY VISWANATHAMURTHI^{*†}, SHANMUGAM SURESH[‡], RAJU NANDHAKUMAR[‡] and TAKESHI HASHIMOTO[§]

[†]Department of Chemistry, Periyar University, Salem-636 011, India

[‡]Department of Chemistry, Karunya University, Karunya Nagar, Coimbatore - 641 114, India

[§]Department of Materials and Life Sciences, Faculty of Science and Technology, Sophia University, 7-1 Kioi-cho, Chiyoda-ku, Tokyo 102-8554, Japan

We report herein synthesis and characterization of four new organoruthenium(II) complexes of the type $[\text{RuH}(\text{CO})(\text{PPh}_3)_2(\text{L}_{1,2})]\text{Cl}$ (**1**, **3**) and $[\text{Ru}(\text{CO})(\text{Cl})_2(\text{AsPh}_3)(\text{L}_{1,2})]$ (**2**, **4**) derived from the reaction of $[\text{RuHCl}(\text{CO})(\text{EPh}_3)_3]$ (E = P or As) with 2-(pyridine-2yl)benzoxazole (**L**₁) and 2-(pyridine-2yl)benzthiazole (**L**₂). Single-crystal X-ray diffraction data of **2** proved octahedral geometry of the complexes with a 1:1 ratio between the metal and the coordinated ligands. The binding affinities of **1-4** toward calf-thymus DNA (CT-DNA) and BSA were thoroughly studied by various spectroscopic techniques. Furthermore, the coordination compounds exhibit catecholase-like activities in the aerial oxidation of 3,5-di-tert-butylcatechol to the corresponding *o*-quinone and phosphatase-like activities in the hydrolysis of 4-nitrophenyl phosphate to 4-nitrophenolate ion. The kinetic parameters have been determined using Michaelis–Menten approach. The highest k_{cat} values suggested that coordination compounds exhibit higher rates of catalytic efficacy.

Keywords: Ruthenium(II) compound; X-ray structure; DNA/BSA binding; Enzyme kinetic studies

1. Introduction

*Corresponding author. Email: viswanathamurthi72@gmail.com

Design and synthesis of small synthetic systems that distinguish specific sites of DNA are essential areas of current research. Such investigations deliver insights for the mechanism of action of antitumor activity [1-6]. Towards this direction, there is a continuing search for new metal compounds that strongly interact with DNA [7-9]. Furthermore, investigation of the interaction of transition metal compounds with DNA helps in the development of new agents that are potentially useful in molecular biology and also in the design of reputed drugs [10-16]. Moreover, strong evidence has been accumulated, showing that metal-to protein interactions are also extremely important in promoting the anticancer activity of transition metal compounds and it has been demonstrated that such interactions could occur with metal ions in either oxidation states [17-24]. In this regard, ruthenium is the most attractive metal owing to its chemical and air stability, structural diversity, low toxicity and ability to mimic iron binding in biological systems, which finally supported ruthenium compounds as highly potent anticancer agents rather than platinum-based drugs [25-29]. The platinum compounds such as cisplatin and carboplatin are still hindered by clinical problems, including acquired or intrinsic resistance, limited spectrum of activity, and high toxicity leading to side-effects. The entrance of two ruthenium-based drugs, NAMI-A and KP1019, into clinical trials for the treatment of metastatic tumors also increased the interest in this metal [30, 31].

Subsequently, many effective biological systems based on ruthenium have been developed because of the fascinating reactivities exhibited by the resultant compounds and the nature of the ligands that dictate the property of these compounds [32-34]. In this regard, benzoxazole/benzthiazole ligands have potential biological applications, and hence their metal compounds exhibit diverse pharmacological applications, due to the structural similarity of benzoxazole/benzthiazole nucleus with natural compounds [35-37].

On the other hand, catechol oxidase (CO) is a member of the type-III copper proteins, which catalyzes the oxidation of catechols to quinones, highly reactive intermediates that undergo auto-polymerization to produce melanin, a brown pigment responsible for protecting damaged tissues against pathogens and insects of higher plants [38-40]. Researchers have focused on dinuclear systems to match the original enzyme structurally, where there exists a dimeric copper active center. Recent investigations have shown that some manganese(II/III), nickel(II), copper(II), zinc(II) and cobalt(II/III) species can also mediate such catechol oxidation [41, 42]. Similarly, catalytic cleavage of phosphate esters either by hydrolysis or *trans*

esterification process has received significant attention as an important biochemical process, *e.g.* hydrolysis of amino-acid esters by esterases, peptides by peptidases, and phosphate esters by phosphoesterases. Earlier investigations showed that dinuclear zinc(II), iron(II), copper(II) compounds were used as mimic catalysts for hydrolysis reaction [43-48]. Therefore, design and synthesis of functional models for catechol oxidase/phosphatase hydrolysis containing metal ions other than copper, say ruthenium, seem to be interesting and at the same time challenging.

Based on the above facts and considering the role and activity of ruthenium and its coordination compounds in biological systems, along with the significance of benzoxazole/thiazole in medicine, we report in this work a systematic study on the synthesis, the structural characterization of organoruthenium(II) complexes containing benzoxazole/thiazole ligands and their interaction with nucleic acids (DNA) and proteins together with catecholase/phosphatase-like activities.

2. Experimental

2.1. Materials

All reagents and solvents were of analytical grade except those employed in photophysical experiments, which were of spectroscopic grade. Doubly distilled water was used to prepare all buffers. Calf-thymus DNA (CT-DNA), bovine serum albumin (BSA) and 4-nitrophenyl phosphate disodium salt hexahydrate (4-NPP) were obtained from Himedia. Ethidium bromide (EB) and 3,5-di-*tert*-butylcatechol (3,5-DTBC) were purchased from Sigma-Aldrich.

2.2. General methods

Elemental analysis (C, H, N, S) were carried out on a Vario EL III CHNS analyzer. Infrared spectra were recorded as KBr pellets using a Perkin-Elmer FT-IR spectrophotometer from 4000-400 cm^{-1} . Electronic spectra were obtained on a JASCO V-570 spectrophotometer. ^1H , ^{13}C and ^{31}P NMR spectra were recorded at room temperature with a Bruker AV400 instrument with chemical shifts relative to tetramethylsilane (^1H , ^{13}C) and *o*-phosphoric acid (^{31}P). Mass spectra for the coordination compounds were performed on an advanced Q-TOF microTM mass spectrometer using electro-spray ionization probe. All MS results are given in the form: *m/z*, assignment. Fluorescence spectral data were performed on a JASCO FP-8200 fluorescence spectrophotometer at room temperature. Single crystal X-ray diffraction data collections were

carried out at 93.0(5) K on a Rigaku AFC8-CCD diffractometer. Melting points were checked on a technico micro heating apparatus and are uncorrected. Stock solutions of compounds (1.0×10^{-4} M in DMF) were stored at 4 °C and required concentrations were prepared for all experiments. All the stock solutions used after no more than four days. Solutions of compounds were prepared freshly 1 h prior to biochemical evaluation. Data have been expressed as the mean \pm standard deviation from three independent experiments.

2.3. Synthesis of ligands (L_1 and L_2)

The ligands 2-(2-pyridyl)benzoxazole (L_1) and 2-(2-pyridyl)benzothiazole (L_2) were prepared according to reported methods [49].

2-(2-pyridyl)benzoxazole (L_1), Yield: 75% (0.213 mg); Color: Yellowish orange; m.p: 130 °C; Micro analytical data for $C_{12}H_8N_2O$: C, 73.46; H, 4.41; N, 14.28%. Found: C, 73.21; H, 4.18; N, 14.12%. IR (KBr, cm^{-1}): 1608, $\nu(C=N_1)_{oxazole}$; 1572, $\nu(C=N_2)_{phenyl}$; 1085, $\nu(C-O)$. UV-vis [CH_2Cl_2 , λ_{max} , nm]: 248, 305. 1H NMR (300.13 MHz; $CDCl_3$, ppm): 8.72 (d, 1H, $J=4.5$), 7.56 (t, 1H, $J=4.4$), 7.75 (t, 1H, $J=6.5$), 7.80 (d, 1H, $J=6.1$), 8.26 (d, 1H, $J=7.8$), 7.72 (t, 1H, $J=5.5$), 7.31 (t, 1H, $J=5.1$), 7.36 (d, 1H, $J=5.8$).

2-(2-pyridyl)benzothiazole (L_2), Yield: 78% (0.245 mg); Color: Yellowish orange; m.p: 123 °C; Micro analytical data for $C_{12}H_8N_2S$: C, 67.90; H, 3.80; N, 13.30; S, 15.11%. Found: C, 67.73; H, 3.61; N, 13.12; S, 15.34%. IR (KBr, cm^{-1}): 1623, $\nu(C=N_1)_{thiazole}$; 1452, $\nu(C=N_2)_{phenyl}$; 1075, $\nu(C-O)$. UV-vis [CH_2Cl_2 , λ_{max} , nm]: 314, 235. 1H NMR (300.13 MHz; $CDCl_3$, ppm): 8.66 (d, 1H, $J=4.6$), 7.52 (t, 1H, $J=7.4$), 7.83 (t, 1H, $J=7.5$), 8.10 (d, 1H, $J=8.1$), 8.32 (d, 1H, $J=7.8$), 7.44 (t, 1H, $J=7.9$), 7.35 (t, 1H, $J=6.3$), 7.94 (d, 1H, $J=7.8$).

2.4. Synthesis of ruthenium(II) complexes 1-4

2.4.1. $[RuH(CO)(PPh_3)_2(L_1)]Cl$ (1). A solution of $[RuHCl(CO)(PPh_3)_3]$ (0.100 g, 0.105 mmol) in ethanol (20 mL) was treated with L_1 (0.0481 g, 0.105 mmol) and the mixture was gently refluxed for 6 h. The reaction was monitored by thin-layer chromatography (TLC) using silica gel coated glass plates with 2:8 mixture of ethyl acetate/petroleum ether as the mobile phase. After the reaction was completed, the resulting solution was cooled to room temperature, the suspension was filtered and the solid was thoroughly washed with cold ethanol and diethyl ether. Yield: 80% (0.124 mg); m.p: 220 °C; Micro analytical data for $C_{49}H_{39}N_2O_2P_2Ru$: C, 69.16; H,

5.80; N, 3.29%. Found: C, 69.35; H, 5.58; N, 3.12%. IR (KBr, cm^{-1}): 1632, $\nu(\text{C}=\text{N}_1)_{\text{oxazole}}$; 1463, $\nu(\text{C}=\text{N}_2)_{\text{phenyl}}$; 1069, $\nu(\text{C}-\text{O})$; 1945, $\nu(\text{C}\equiv\text{O})$; 1474, $\nu(\text{C}-\text{CH})_{\text{in-plane}}$; 1432, $\nu\{\text{Ph}(\text{P}-\text{Ph})\}$. UV-vis [CH_2Cl_2 , λ_{max} , nm]: 235, 275, 438. ^1H NMR (300.13 MHz; $\text{DMSO}-d_6$, ppm): 7.95–7.73 (m, 4H, Ar H), 7.69–7.44 (m, 8H, Ar H), 7.33–7.09 (m, 12H, Ar H), 6.87–6.68 (t, 8H, Ar H), 6.55–6.51 (m, 7H, Ar H) -6.82 (s, 1H, Ru-H). ^{13}C NMR (100 MHz, CDCl_3 , ppm): 205.73 ($\text{C}\equiv\text{O}$), 138.12 (Ar C), 137.33 (Ar C), 137.14 (Ar C), 136.15 (Ar C), 135.80 (Ar C), 135.65 (Ar C), 133.54 (Ar C), 133.46 (Ar C), 132.84 (Ar C), 128.97 (Ar C), 128.43 (Ar C), 128.15 (Ar C), 127.95 (Ar C), 127.69 (Ar C), 127.15 (Ar C), 126.84 (Ar C). ^{31}P NMR (162 MHz, CDCl_3 , ppm) 30.15. MS (ESI, m/z): 849.2 $[\text{M}]^+$.

2.4.2. Synthesis of $[\text{RuCl}_2(\text{CO})(\text{AsPh}_3)(\text{L}_1)]$ (2). **2** was prepared by adopting the procedure used for the synthesis of **1** by reacting $[\text{RuHCl}(\text{CO})(\text{AsPh}_3)_3]$ with L_1 in 20 mL of $\text{MeOH}/\text{CHCl}_3$ (1:1 v/v) solvent mixture. Yield: 75% (0.086 mg); m.p: 180 °C; Micro analytical data for $\text{C}_{31}\text{H}_{23}\text{N}_2\text{O}_2\text{Cl}_2\text{AsRu}$: C, 53.00; H, 3.30; N, 3.98%. Found: C, 53.18; H, 3.11; N, 3.72%. IR (KBr, cm^{-1}): 1634, $\nu(\text{C}=\text{N}_1)_{\text{oxazole}}$; 1448, $\nu(\text{C}=\text{N}_2)_{\text{phenyl}}$; 1052, $\nu(\text{C}-\text{O})$; 1934, $\nu(\text{C}\equiv\text{O})$; 1497, $\nu(\text{C}-\text{CH})_{\text{in-plane}}$; 1423, $\nu\{\text{Ph}(\text{As}-\text{Ph})\}$. UV-vis [CH_2Cl_2 , λ_{max} , nm]: 239, 272, 347. ^1H NMR (300.13 MHz; $\text{DMSO}-d_6$, ppm): 7.86–7.63 (m, 4H, Ar H), 7.57–7.41 (m, 4H, Ar H), 7.38–7.12 (m, 4H, Ar H), 6.84–6.53 (m, 6H, Ar H), 6.37–6.13 (m, 5H, Ar H). ^{13}C NMR (100 MHz, CDCl_3 , ppm): 207.24 ($\text{C}\equiv\text{O}$), 137.52 (Ar C), 136.85 (Ar C), 136.72 (Ar C), 134.85 (Ar C), 133.72 (Ar C), 132.63 (Ar C), 131.58 (Ar C), 130.43 (Ar C), 130.12 (Ar C), 129.57 (Ar C), 128.94 (Ar C), 127.45 (Ar C), 125.2 (Ar C). (ESI, m/z): 665.8 $[\text{M}-\text{Cl}]^+$. Single crystals suitable for X-ray determination were grown by slow evaporation of methanol/chloroform solution of **2** at room temperature.

2.4.3. Synthesis of $[\text{RuH}(\text{CO})(\text{PPh}_3)_2(\text{L}_2)]\text{Cl}$ (3). **3** was prepared by adopting the procedure used for the synthesis of **1** by reacting $[\text{RuHCl}(\text{CO})(\text{PPh}_3)_3]$ with L_2 . Yield: 82% (0.093 mg); m.p: 193 °C; Micro analytical data for $\text{C}_{49}\text{H}_{39}\text{N}_2\text{OSP}_2\text{Ru}$ required: C, 67.88; H, 4.53; N, 3.23; S, 3.70%. Found: C, 67.59; H, 4.21; N, 3.02; S, 3.51%. IR (KBr, cm^{-1}): 1638, $\nu(\text{C}=\text{N}_1)_{\text{thiazole}}$; 1434, $\nu(\text{C}=\text{N}_2)_{\text{phenyl}}$; 1072, $\nu(\text{C}-\text{O})$; 1962, $\nu(\text{C}\equiv\text{O})$; 1495, $\nu(\text{C}-\text{CH})_{\text{in-plane}}$; 1417, $\nu\{\text{Ph}(\text{P}-\text{Ph})\}$. UV-vis [CH_2Cl_2 , λ_{max} , nm]: 237, 281, 418. ^1H NMR (300.13 MHz; $\text{DMSO}-d_6$, ppm): 7.86–7.80 (m, 4H, Ar H), 7.78–7.64 (m, 8H, Ar H), 7.55–7.32 (m, 14H, Ar H), 6.84–6.52 (m, 12H, Ar H) -6.04 (s,

1H, Ru-H). ¹³C NMR (100 MHz, CDCl₃ ppm): 208.31 (C≡O), 139.20 (Ar C), 138.93 (Ar C), 138.81 (Ar C), 138.67 (Ar C), 136.75 (Ar C), 136.12 (Ar C), 133.74 (Ar C), 132.52 (Ar C), 131.67 (Ar C), 129.72 (Ar C), 128.78 (Ar C), 128.63 (Ar C), 127.82 (Ar C), 127.64 (Ar C), 126.92 (Ar C), 126.44 (Ar C). ³¹P NMR (162 MHz, CDCl₃, ppm) 29.32. MS (ESI, *m/z*): 865.1 [M]⁺.

2.4.4. Synthesis of [RuCl₂(CO)(AsPh₃)(L₂)] (4). **4** was prepared by adopting the procedure used for the synthesis of **2** by reacting [RuHCl(CO)(AsPh₃)₃] with L₂. Yield: 75% (0.856 mg); m.p: 188 °C; Micro analytical data for C₃₁H₂₃N₂OSCl₂AsRu: C, 51.82; H, 3.20; N, 3.89; S, 4.46%. Found: C, 51.58; H, 3.06; N, 3.68; S, 4.24%. IR (KBr, cm⁻¹): 1639, ν(C=N₁)_{thiazole}; 1442, ν(C=N₂)_{phenyl}; 1063, ν(C-O); 1931, ν(C≡O); 1482, ν(C-CH)_{in-plane}; 1421, ν{Ph(As-Ph)}. UV-vis [CH₂Cl₂, λ_{max}, nm]: 238, 282, 333, 355, 470. ¹H NMR (300.13 MHz; DMSO-*d*₆, ppm): 7.94–7.85 (m, 4H, Ar H), 7.67–7.44 (m, 4H, Ar H), 7.39–7.17 (m, 4H, Ar H), 6.95–6.52 (m, 6H, Ar H), 6.48–6.16 (m, 5H, Ar H). ¹³C NMR (100 MHz, CDCl₃, ppm): 207.17 (C≡O), 139.69 (Ar C), 138.84 (Ar C), 138.24 (Ar C), 134.55 (Ar C), 130.92 (Ar C), 129.54 (Ar C), 128.81 (Ar C), 128.31 (Ar C), 127.70 (Ar C), 126.14 (Ar C), 126.54 (Ar C), 125.68 (Ar C), 124.32 (Ar C). (ESI, *m/z*): 717.2 [M-Cl]⁺.

2.5. X-ray structure determination

Crystals of **2** were mounted on a glass fiber and used for data collection. The crystal data were collected at 93.0(5) K using a Rigaku AFC8-CCD diffractometer. Mo-Kα radiation (0.7170 Å) was used throughout for studies. The absorption corrections were performed by the multi-scan method. Corrections were made for Lorentz and polarization effects. Structure solutions and refinements were performed using the programs SHELXS-2014 [50, 51]. The structure was solved by direct-methods to locate the heavy atoms, followed by difference maps for the light non-hydrogen atoms. Details of the data collection and refinement are gathered in table 1 and important bond lengths and angles are summarized in table 2.

2.6. DNA-binding studies

2.6.1. Emissive titration. Fluorescence spectral titrations were performed at room temperature in Tris-HCl/NaCl buffer (5 mM Tris-HCl/50 mM NaCl buffer, pH 7.2) to investigate the binding

affinity between CT-DNA and complexes. Mixing of such solutions with the aqueous buffer DNA solutions used in the studies never exceeded 5% DMSO (v/v) in the final solution, which was needed due to low aqueous solubility of most of the compounds. The CT-DNA concentration per nucleotide was determined using fluorescence spectrometry by the complexes excitation wavelength. During titration, an equal quantity of CT-DNA was added to both the complexes solution and reference solution to eliminate the intensity of CT-DNA itself and the Tris-HCl/NaCl buffer was subtracted through baseline correction. Emissive titration experiments were performed with a fixed concentration of **1-4** (25 μM). While gradually increasing the concentration (0-50 μM) of DNA, the emission intensities were recorded for coordination compounds in the range of 350-650 nm. Titrations were manually done by a micropipette for the addition of CT-DNA.

2.6.2. EB-displacement assay. DNA binding tendency of the ruthenium complexes also were measured by the fluorescence based EB displacement studies. EB-displacement experiments were achieved by observing changes in the fluorescence intensity on the emission wavelength at $\lambda_{\text{emis}} = 602$ nm at the excitation wavelength at $\lambda_{\text{ex}} = 500$ nm, after aliquot addition of coordination compounds to an aqueous solution of the EB-DNA. EB alone showed minimal fluorescence and the fluorescence was enhanced significantly with gradual addition of CT-DNA until maximum fluorescence was attained due to the formation of an intercalative DNA-EB adduct. Before the emission spectra were recorded, CT-DNA was pretreated with EB in the ratio $[\text{DNA}]/[\text{EB}] = 1$ and kept for 30 min at room temperature in order to fully react. Then, the complexes were added to this mixture of EB-DNA by manual titration and the changes in the fluorescence intensity were noted down.

2.6.3. Viscosity experiment. Viscosity measurement was carried out using an Ubbelodhe viscometer immersed in a thermostatic water bath maintained at 25 ± 0.1 °C. DNA samples with approximately 200 base pairs in length were prepared by sonication in order to minimize the complexities arising from DNA flexibility. Flow times were measured with a digital stopwatch; each sample was measured three times at 5 min interval, and an average flow time was calculated. Relative viscosities for CT-DNA in the presence and absence of the complexes were calculated from the relation $\eta = (t-t_0)/t_0$, where t is the observed flow time of DNA-containing

solution and t_0 is the flow time of Tris–HCl/NaCl buffer alone. Data are presented as $(\eta/\eta_0)^{1/3}$ versus binding ratio, where η is the viscosity of CT-DNA in the presence of the complex and η_0 is the viscosity of CT-DNA alone.

2.7. Protein binding study

The binding mode of **1-4** with BSA was performed using the fluorescence spectra at room temperature with an excitation wavelength of BSA at 280 nm and monitoring the emission at 344 nm by keeping the concentration of BSA constant (2.5 μM) while increasing the complexes concentration (0-50 μM) regularly. The excitation and emission slit widths (each 5 nm) remained constant for all the experiments. A scan rate of 200 nm min^{-1} was used. In addition, absorption titration experiments were carried out by keeping the concentration of the coordination compounds (20 μM) and the BSA concentration (2.5 μM) as constant. Furthermore, the type of quenching mechanism of coordination compounds was determined from the UV-visible absorption spectra in the range of 200-600 nm.

2.8. Catalytic oxidation of 3,5-DTBC

The kinetic experiments were carried out using fluorescence quenching spectra under pseudo first-order conditions. Quenching of the emission intensity of 3,5-DTBC at $\lambda_{\text{emis}} = 440$ nm ($\lambda_{\text{ex}} = 401$ nm) was monitored by addition of the complexes. The compounds (1×10^{-4} M) in DMF were added to 100 equivalents of 1×10^{-3} M solutions of 3,5-DTBC in DMF at aerobic conditions. Emissive intensity of the resultant reaction mixture was plotted with respect to wavelength at a regular interval of 15 min in a fluorescence spectrophotometer in the range of 400-700 nm. The dependence of the rate on substrate concentration and different kinetic parameters were obtained by treatment of coordination compounds with 3,5-DTBC and monitoring the increase in emission intensity at 440 nm (the peak corresponding to the quinone band maxima) as a function of time.

2.9. Phosphate ester hydrolysis

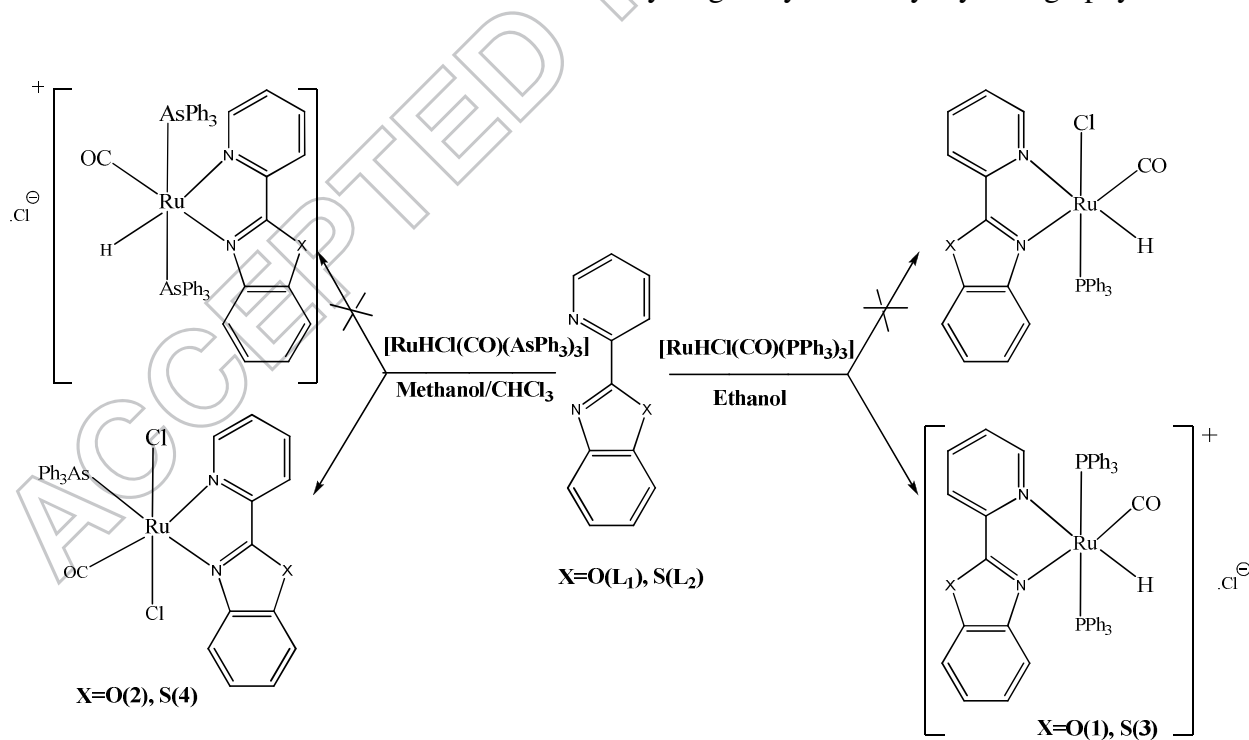
The hydrolysis of 4-NPP catalyzed by ruthenium compounds at room temperature was studied using fluorescence quenching spectroscopy. The hydrolytic tendency was detected spectrophotometrically by monitoring the time evolution of *p*-nitrophenolate in DMF ($\lambda_{\text{max}} =$

465 nm) through a wavelength scan from 410–700 nm over 2 h. Quenching of the emission intensity of 4-NPP at 465 nm (excitation wavelength at 401 nm) was monitored using **1-4**. The hydrolase activity involves the preparation of stock solutions of compounds (0.05×10^{-3} M) and the substrate 4-NPP (1×10^{-3} M), at higher concentrations in pure DMF. The dependence of the rate on substrate concentration and different kinetic parameters were obtained by treatment of 0.05×10^{-3} M solution of coordination compounds with 40 equivalents of substrate (the peak corresponding to the phenolate band maxima) as a function of time.

3. Results and discussion

3.1. Synthesis

L_1 and L_2 were synthesized through the condensation reaction of picolinic acid and 2-aminophenol or 2-aminothiophenol in polyphosphoric acid according to the previous reported procedures. The ligands react with 1:1 ratio amount of ruthenium precursor complexes in ethanol or methanol/chloroform mixture to form the corresponding ruthenium complexes **1-4**. The unprecedented formation of **1-4** is shown in scheme 1. The ligands and their complexes were characterized by elemental analysis, FT-IR, UV-vis, NMR and ESI-mass spectral techniques. In addition molecular structure of **2** was confirmed by single-crystal X-ray crystallography.



Scheme 1. Synthesis of organoruthenium(II) complexes **1-4**.

3.2. Structural characterization

The IR spectra provide valuable information regarding the nature of the functional group attached to the metal atom. The coordinated stretching vibration bands were assigned by comparing the IR spectra of the free ligands with the spectra of their metal complexes. A strong band was observed at 1623-1608 cm^{-1} in the ligands corresponding to oxazole/thiazole ring C=N which was shifted to 1639-1632 cm^{-1} in the complexes indicated the participation of oxazole/thiazole ring nitrogen in bonding. The pyridine ring (C=N) appeared as sharp peak at 1572-1452 cm^{-1} in free ligands, shifted to lower frequency 1463-1412 cm^{-1} in all complexes indicated that pyridine ring nitrogen is coordinated to central metal. The band in the range 1962-1931 cm^{-1} was attributed to the stretching mode of the C \equiv O group present in the complexes [52, 53]. In addition, bands appearing in the region 1497-1474 cm^{-1} in the spectra of complexes were assigned to -C-CH in the plane stretching vibration. The bonding between ligand and metal was also confirmed by the presence of new bands at 548-425 cm^{-1} in complexes resulting in the M-N (metal–nitrogen) vibration [54].

The UV-vis spectra were recorded in DMSO solution. The free ligand showed two intense bands around 235-314 nm which were assigned to intra-ligand transitions of the type $\pi \rightarrow \pi^*$ and $n \rightarrow \pi^*$. The spectra of the complexes showed bands around 238-353 nm which might be assigned to ligand-to-metal charge-transfer transition (LMCT) [55]. The low intensity band in the region 418-470 nm in the complexes is assigned to metal-to-ligand charge-transfer transition (MLCT) (figure S1). The pattern of the electronic spectra of the complexes indicated the presence of an octahedral environment around ruthenium(II) ion similar to other ruthenium complexes [56, 57].

The ^1H NMR spectra of the ligands and their complexes were recorded to confirm the binding of ligand to the metal ion. The spectra of free ligands and their corresponding coordination compounds showed peaks for aromatic protons in the region 6.13-8.72 ppm (figures S2 and S3). The hydride ligand signal has been observed in the high field region at -6.82 and -6.04 ppm for **1** and **3** which indicated the complexes **1** and **3** having Ru-H bond, while in complexes **2** and **4**, there is no Ru-H bond [58] (figures S4-S7). ^{13}C NMR spectra of the coordination compounds showed a peak at 208.3-205.7 ppm due to carbonyl carbon (C \equiv O)

present in all complexes. The presence of peak at 139.69-137.52 ppm was assigned to oxazole/thiazole ring C=N group. The aromatic carbon showed their peaks in the region 138.84-136.85 ppm [59] (figures S8-S11). ^{31}P NMR spectra of **1** and **3** were recorded to confirm the presence of triphenylphosphine group and their geometry in the complexes. A sharp singlet was observed around 29.32–30.15 ppm, due to the presence of two magnetically equivalent triphenylphosphine ligands coordinated in *trans* position [60] (figure S12).

The ESI-MS spectra of coordination compounds were recorded to confirm their molecular ions. Complexes **1** and **3** exhibited the molecular ion peaks at m/z 849.2 and 865.1, respectively, which were assigned to $[\text{M}]^+$ ions and **2** and **4** showed peaks at m/z 665.8 and 717.2, respectively, which were assigned to $[\text{M-Cl}]^+$ (figures S13-S16). The obtained molecular masses are in agreement with the calculated molecular masses.

The crystal structure of **2** along with the numbering scheme is given in figure 1. The crystallographic data and structure refinement parameters for **2** are summarized in table 1 and selected bond lengths and angles are depicted in table 2. The unit cell packing diagram for **2** is given as figure S17. Single-crystal X-ray studies revealed that **2** crystallized in triclinic crystal system with space group *P*-1. Complex **1** was formed as a cationic complex in which the chloride ion presents as counter ion in the outside of the coordination spheres (see Supporting Information, figures S18 and S19).

Complex **2** was expected as a cationic complex similar to **1**. Nevertheless, **2** was formed as a neutral complex due to the solvent (CHCl_3) assisted formation according to the Riemer-Tiemann reaction mechanism. In **2**, the basal plane consists of pyridine nitrogen, oxazole nitrogen of the ligand in its neutral bidentate fashion, one triphenylarsine group and carbonyl group. The other coordination sites were filled up by two chloride atoms which are present in *trans* position. The bidentate pyridyl chelate ligand coordinated equatorially to the metal ion with the formation of five-membered ring with the bite angle N(5)-Ru(1)-N(2) is $76.13(12)^\circ$. The only one triphenyl arsine group occupies the *cis* position of the chlorine ligand, the bond angle Cl(1)-Ru(1)-As(1) is $95.45(7)^\circ$. The equatorial bond lengths are [Ru(1)-N(2)] 2.120(4) Å, [Ru(1)-N(5)] 2.234(3) Å, [Ru(1)-C(1)] 1.829(4) Å and [Ru(1)-As(1)] 2.3974(19) Å, and the axial bond lengths are [Ru(1)-Cl(1)] 2.4630(18) Å and [Ru(1)-Cl(2)] 2.397(2) Å and are comparable with the distances found in previously reported ruthenium complexes [61-65]. Carbonyl group (CO) occupies the *trans* site to the pyridine ring. This may be a consequence of Ru→CO back

donation as indicated by the short Ru(1)-C(16) [1.848(4) Å] (**1**) and Ru(2)-C(32) [1.834(2) Å] (**2**) bonds and low stretching frequency, which preferred weak σ - or π -donors occupying the opposite site to CO favor the back donation. The bonding parameters around the ruthenium center confirm a slightly distorted octahedral geometry and are in a comparable range to those of the closely related ruthenium complexes in the literature [66-68]. Unfortunately, the high-quality crystals of **3** and **4** suitable for X-ray single-crystal diffraction have not been obtained, suggesting that refined structural factors are critical to stabilize these species. But the similarities in their spectroscopic characteristics suggest that **1** is a good structural model for **3** and **2** is structural model for **4**.

3.3. DNA binding studies

3.3.1. Stability of compounds. Before carrying out DNA-binding studies, the stability of **1-4** was checked by UV-vis absorption spectra. The spectra for the complexes in the presence of Tris-HCl/NaCl buffer at four different time points (0 min, 1 h, 6 h and 12 h) were recorded. The spectral results did not reveal any noticeable change in either the intensity or the position of the absorption bands in Tris-HCl/NaCl buffer solution. These results established that the complexes retain a stable structure under physiological conditions (figure S1).

3.3.2. Fluorescence emission technique. In general the interaction of metal compounds with DNA takes place *via* both covalent and non-covalent interaction. In the case of covalent binding, the labile ligand of the complexes is replaced by a nitrogen of DNA-base, whereas in non-covalent interactions, the metal complexes interact with the outside of the DNA-helix. Emissive spectroscopy is an effective method to examine the binding mode of metal compounds with DNA and its magnitude. The emission spectra of **1-4** at fixed concentration (25 μ M) is titrated with varying amounts of DNA (0-50 μ M) were recorded. Then, aliquot addition of CT-DNA to metal complexes leads to continual hypochromism (19.1% for **1**, 12.8% for **2**, 19.27% for **3**, 19.3% for **4**) with red-shift of 2-3 nm (figures 2 and S20). The observed hypochromism is due to an intercalative mode of binding involving a strong stacking interaction between extended aromaticity of the ligands and the DNA-base pairs. The binding of complexes to DNA leads to hypochromism, which provides a measure of the strength of the intercalation. In order to determine quantitatively the binding strength of the complexes with CT-DNA, intrinsic binding

constants (K_{bin}) were obtained by monitoring the changes in the wavelength and the corresponding intensity of emission of **1-4**. The binding constant was obtained by the following Scatchard equation [69],

$$C_F = C_T[I/I_0 - P]/[1 - P] \quad (1)$$

where C_T is the concentration of the complex added, C_F is the concentration of the free complex, I_0 , I were its emission intensities in the absence and presence of DNA, respectively, and P is the ratio of the observed emission quantum yield of the bound complex to the free complex. The value of P was obtained from a plot of I/I_0 vs $1/[DNA]$ such that the limiting emission yield is given by their intercept. The amount of bound complex C_B at any concentration was equal to $C_T - C_F$. The obtained Scatchard plots of r/C_F versus r for tested compounds with increasing concentration of CT-DNA are depicted in figure S21. A plot of r/C_F versus r ($= C_B/[DNA]$) gives the intrinsic binding constant K_{bin} and the values are listed in table 3. From the results, it has been concluded that the complexes bind to DNA via intercalative mode [70-75]. The K_{bin} values for **1**, **2**, **3** and **4** were 4.16×10^4 , 4.83×10^4 , 4.50×10^4 and $4.99 \times 10^4 \text{ M}^{-1}$, respectively, which were lower than the K_{bin} values reported for $[Ru(dmb)_2(ipad)](ClO_4)_2$ ($2.2 \times 10^6 \text{ M}^{-1}$), $[Ru(dmp)_2(ipad)](ClO_4)_2$ ($1.0 \times 10^6 \text{ M}^{-1}$), $[Ru(dip)_2(ipad)](ClO_4)_2$ ($0.5 \times 10^6 \text{ M}^{-1}$) [71], but comparable with $[Ru(bpy)_2(L^1)](PF_6)_4 \cdot CH_3OH$ ($5.7 \times 10^4 \text{ M}^{-1}$), $[Ru(bpy)_2(L^2)](PF_6)_4 \cdot 2H_2O$ ($4.1 \times 10^4 \text{ M}^{-1}$) [76], and larger than those for *cis*- $[Ru(bpy)_2(OFX)]Cl \cdot 2H_2O$ ($1.12 \times 10^4 \text{ M}^{-1}$), *cis*- $[Ru(dmbpy)_2(OFX)]Cl \cdot 2H_2O$ ($1.78 \times 10^4 \text{ M}^{-1}$), *cis*- $[Ru(phen)_2(OFX)]Cl \cdot 2H_2O$ ($2.36 \times 10^4 \text{ M}^{-1}$) [77]. The stronger binding affinity of **4** and **2** might be due to slightly longer Ru–As bond distance when compared to Ru–P bond distance in **3** and **1**, which affects how far the aromatic chromophore would be able to intercalate into the DNA. The Ru–P distance of 2.3738(6) Å is about 0.09 Å, shorter than the Ru–As bond of 2.4630(8) Å, which places the phenyl rings of the PPh₃ or AsPh₃ units closer to the aromatic chromophore by this distance value for the compounds containing PPh₃, thus hindering further intercalation of the chromophore into the DNA due to steric interaction with the phenyl groups. For compounds containing AsPh₃, the phenyl groups are further removed from the chromophore, thus allowing for a slightly deeper intercalation accompanied by more pronounced π -stacking interactions between the chromophore and the DNA-bases resulting in ultimately a slightly higher intrinsic binding constant [78]. Moreover, the complexes containing benzthiazole ligand showed slightly higher

binding ability than the complexes containing benzoxazole ligand [79].

3.3.3. EB-displacement study. Usually, competitive binding experiments were carried out using metal complexes as a quencher, which provide strong information about the binding of the complexes to DNA. EB is widely used as sensitive fluorescence probe for native DNA. It emits intense fluorescent light in the presence of DNA due to strong intercalative interaction between the adjacent DNA base pair [80]. Interaction of **1-4** with CT-DNA in EB solution leads to substantial quenching in fluorescence intensity due to the displacement of EB from EB-DNA adduct. This displacement technique is based on the decrease of fluorescence intensity resulting from the displacement of bound EB from a DNA sequence by a quencher and the quenching is due to the reduction of the number of binding sites on the DNA that is available for EB. Hence, this method serves as indirect evidence to identify intercalative binding modes. While adding increasing concentration of **1-4** (0-50 μM) to fixed concentration of EB-DNA solution (7.5 μM) significant decrease in fluorescence intensity with the hypochromism (39.6% for **1**, 32.6% for **2**, 36% for **3**, 52.2% for **4**) and noticeable red-shift 2-4 nm was observed (figures 3 and S22). From this evidence, it is concluded that EB is being released from EB-DNA compound because of its exchange by corresponding ruthenium complexes. The quenching parameter of **1-4** have been calculated using the Stern-Volmer equation,

$$I_0/I = 1 + K_{sv} [Q] \quad (2)$$

where I_0 and I are the emission intensities of EB bound CT-DNA in the absence and presence of the quencher (complexes) concentration $[Q]$, respectively, which gave the Stern-Volmer quenching constant (K_{sv}). The K_{sv} value is obtained with a slope from the plot of I_0/I versus $[Q]$ which are shown in figure S23. The quenching constant (K_{sv}) values are listed in table 4.

Further, the apparent DNA binding constant (K_{app}) values were also calculated using the following equation:

$$K_{EB} [EB] = K_{app} [M_{50\%}] \quad (3)$$

where $K_{EB} = 1.0 \times 10^7 \text{ M}^{-1}$ is the DNA-binding constant of EB, $[EB]$ is the concentration of EB (7.5 μM) and $[M_{50\%}]$ is the concentration of the compound used to obtain a 50% reduction in

fluorescence intensity of DNA pretreated with EB. The K_{app} value for **1-4** are given in table 4.

3.3.4. Viscosity measurement. Further exploration of the interaction mode between the ruthenium(II) complexes and CT-DNA was carried out by viscosity measurements with a view to discover the DNA-binding properties assessed from the above spectral studies. In general, the viscosity of double-stranded DNA increases when complexes bind DNA in an intercalating mode but remains unchanged when complexes bind in an electrostatic mode; the groove-binders have little effect on DNA-viscosity [81]. From this information, these measurements could provide strong support in favor of intercalative binding. When ruthenium(II) complexes **1-4** were treated with CT-DNA (200 μM), the concentration of complexes (0-120 μM) increased from a ratio of $R = 0-0.1$ ($1/R = [\text{compound}]/[\text{DNA}]$) (figure 4), the relative viscosity of DNA solution exhibited an increase upon addition of the complexes. The observed behavior of DNA-viscosity upon addition of the compounds may be considered as evidence of the existence of an intercalative binding mode to DNA, a conclusion that elucidates the preliminary indications derived from fluorescence spectroscopy studies.

3.4. BSA binding

3.4.1. Fluorescence spectroscopy. Serum albumin is a major transport protein found in the blood plasma. Studies on binding of metal complexes with protein are becoming increasingly important for interpreting the metabolism and transporting process. In the present work, BSA was chosen as model protein due to its structural similarity with human serum albumin. The binding activity of the complexes with serum albumin has been studied from the concentration dependence upon the change in the fluorescence intensity of protein after the addition of complexes [82]. To investigate the interaction mechanism and binding, fluorescence titration experiments have been performed by using BSA (2.5 μM) and varying concentration of ruthenium complexes **1-4** (0-50 μM) at room temperature; the results are illustrated in figures 5 and S24. As seen in the figures, the effect of complexes on the fluorescence intensity of protein at 347 nm show significant trends, indicating that interaction of complexes with BSA could cause the conformational change in the protein structure. To obtain deep insight into the quenching progression, the quenching constant (K_q) was analyzed by the Stern-Volmer equation [69],

$$I_0/I = 1 + K_{sv}[Q] = 1 + K_q \tau_o [Q] \quad (4)$$

where I_0 and I are the fluorescence intensity in the absence and presence of the quencher, respectively, τ_o is the fluorescence life time of BSA ($\tau_o = 10^{-8}$ s), k_q is the quenching rate constant and K_{sv} and $[Q]$ are the Stern-Volmer quenching constant and the concentration of the quencher, respectively. Quenching constants (K_q) have been obtained from the plot of $\log (I_0-I) / I$ versus $\log [Q]$ (figure S25). The quenching parameters of BSA for all the complexes are shown in table 4. The quenching mechanism of the complexes-BSA systems have been proved through following UV-visible spectral study.

3.4.2. UV-vis spectroscopic study. The fluorescence quenching mechanisms are usually classified as either static or dynamic quenching. Static quenching usually results from the formation of a complex between the quencher and the fluorophore in the ground state, whereas in dynamic quenching, the fluorophore and the quencher come into contact with each other during the transient existence of the excited state. The type of quenching can be determined by using UV-vis spectral study. The UV-vis absorption spectra of BSA in the presence of complexes are shown in figure 6. The absorption intensity of BSA was enhanced as the complexes were added, and there was a little blue/red-shift, indicating that the complexes can interact with BSA by static quenching mechanism [83].

3.4.3. Binding constant and binding site number. When static quenching interaction occurs, it is assumed that the complex binds independently to a set of equivalent binding sites in BSA, the binding parameters can be determined according to the Scatchard equation,

$$\log [I_0-I / I] = \log K_{bin} + n \log [Q] \quad (5)$$

where K_{bin} is the binding constant of the compound with BSA and “n” is the number of binding sites. The number of binding sites “n” and the binding constant (K_{bin}) have been found from the plot of $\log (I_0-I) / I$ versus $\log [Q]$ (figure S26). The calculated values of K_q , K_{bin} and “n” values are gathered in table 4. The value of “n”, which is approximately equal to 1, indicates that the binding site in BSA is unique. The higher values of K_q and K_{bin} indicated a strong interaction

between BSA and the complexes.

3.5. Catecholase activity

The catecholase-like activities of the four organoruthenium(II) complexes were determined by the catalytic oxidation of 3,5-DTBC. 3,5-DTBC is chosen as model substrate for this reaction, because its low reduction potential makes it easy to oxidize and bulky tertiary groups present in the compound prevent further oxidation reaction such as ring opening [84]. However, the oxidation product 3,5-DTBQ (3,5-di-tert-butyl quinone) is highly stable and exhibited characteristic emission at λ_{emis} at 440 nm in DMF solvent. Based on the above, the bio-catalytic activity of ruthenium(II) complexes **1-4** for the oxidation of 3,5-DTBC to the corresponding quinone in DMF were carried out at room temperature by fluorescence emission spectroscopy. Catecholase like activities of **1-4** (1×10^{-4} M) were confirmed by adding the complexes to 100 equivalents DMF solution of 3,5-DTBC (1×10^{-2} M) at room temperature under aerobic conditions and the progress of the reaction was studied based on the fluorescence spectra of the mixture at 15 min intervals up to 2 h. Upon addition of 3,5-DTBC, a new band gradually appeared about 400 nm due to the formation of 3,5-DTBQ (figures 7 and S27). Thus, the experiment clearly proves that the oxidation of 3,5-DTBC to 3,5-DTBQ which is catalyzed by the new complexes, as it is well established that 3,5-DTBQ shows a maximum at $\lambda_{\text{emis}} = 440$ nm in pure DMF.

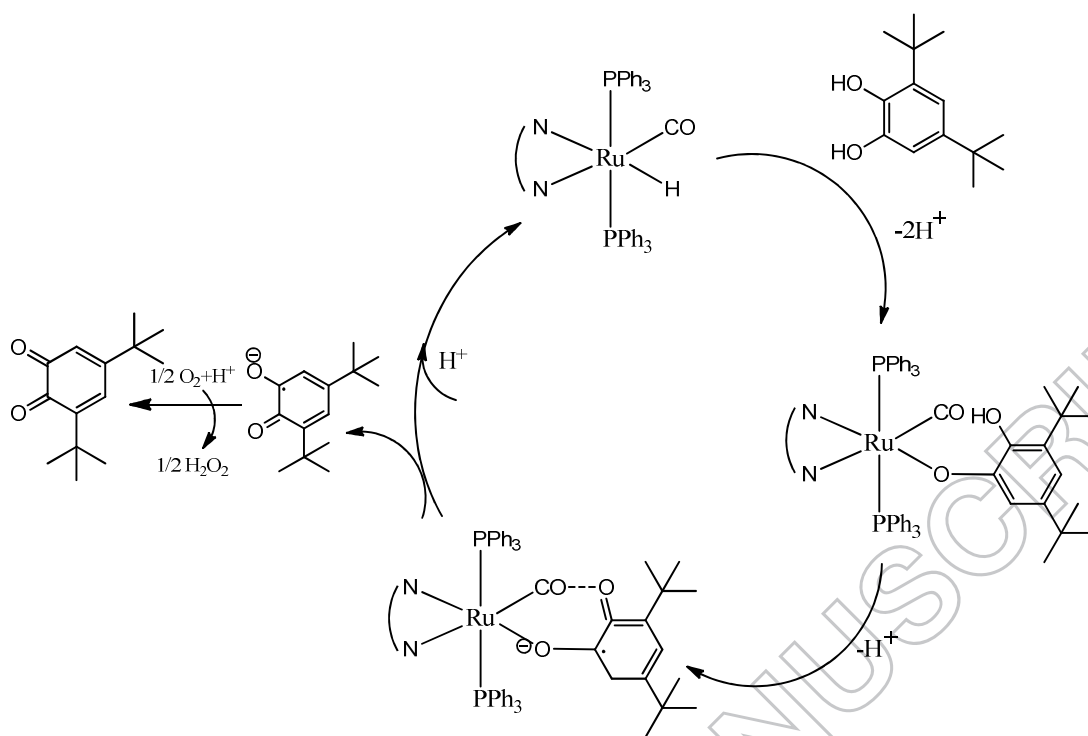
3.5.1. Kinetics of catecholase activity. The kinetics of the oxidation of 3,5-DTBC to 3,5-DTBQ was determined by the method of initial rates [85], following the oxidation product 3,5-DTBQ emission increase at 440 nm. The oxidation rates and various kinetic parameter of the substrate concentration were determined using 10^{-4} M solution of complexes with the different concentration of 3,5-DTBC (10-100 equivalents), under the aerobic condition. In the complexes, a first-order kinetics was observed at low concentration of 3,5-DTBC. However, in higher concentration, saturation kinetics was observed. The catalytic behavior treatment was based on the Michaelis–Menten model seemed to be appropriate under excess substrate conditions [86].



$$v = \frac{v_{max}[S]}{K_M + [S]} \quad (7)$$

$$\frac{1}{v} = \frac{K_M}{v_{max}} \frac{1}{[S]} + \frac{1}{v_{max}} \quad (8)$$

The Michaelis–Menten constant (K_M) and maximum initial rate (V_{max}) were determined by linearization using Lineweaver-Burk plots (figure S29). The observed rate constants k_i were obtained by initial rate method. Plots of k_i versus [3,5-DTBC] gave non-linear curve of decreasing slope. The turnover number (k_{cat}) values can be calculated by dividing the V_{max} values by the concentration of the corresponding complexes as described in table 5. A probable mechanistic for 3,5-DTBC oxidation which was promoted by ruthenium(II) complexes is schematically depicted in scheme 2. Unfortunately, we were unable to characterize the intermediates. After proper workup, when a mixture of starch-potassium iodide solution was added to a mixture of complex and 3,5-DTBC, blue coloration developed, which indicates that hydrogen peroxide was produced during the course of reaction. It is interesting to note that no blue coloration was observed in the absence of 3,5-DTBC. A believable mechanistic path of the formation of H_2O_2 as by product during the oxidation of 3,5-DTBC to 3,5-DTBQ catalyzed complexes was suggested by Chyn and Urbach [87]. It is concluded that **1-4** belong to the highly efficient catalyst group.



Scheme 2. Probable mechanism for oxidation of 3,5-DTBC by complexes.

3.6. Phosphatase activity

The substrate 4-NPP was chosen to study the phosphatase mimic activity of synthesized complexes. Its hydrolytic tendency was distinguished using emissive intensities by monitoring the time evolution of *p*-nitrophenolate ion (4-NP) in DMF at $\lambda_{\text{emis}} = 465$ nm through a wavelength scan from 400-800 nm over 15 min intervals up to 2 h. The emission performances of the complexes are shown in figures 8 and S30.

3.6.1. Kinetic studies. Kinetic studies of phosphatase hydrolysis were performed by the initial-slope method [85], by monitoring the rate of increase in the emissive intensity band at 475 nm, which corresponds to increase in 4-NP concentration. The dependence of the initial rate on the concentration of the substrate was monitored at the respective wavelength by fluorescence emissive spectroscopy. The hydrolytic cleavage (phosphate ester hydrolysis) rate initially increases linearly as the 4-NPP concentration increases but deviates progressively from linearity and finally tends toward saturation curve, and a treatment based on the Michaelis–Menten model seemed to be appropriate under excess substrate conditions. The kinetic parameters such as V_{max} ,

K_M and k_{cat} for the catalyzed reaction were determined from the plots $1/v$ versus $1/[NPP]$ (Lineweaver Burk plot) as per Michaelis-Menten approach for enzymatic kinetics (figure S32). Kinetic parameters of all the complexes are given in table 6. The results indicated first-order rate constant values, which are comparable to the reported values for phosphate bond cleavage [88].

4. Conclusion

A set of four new organoruthenium(II) complexes containing pyridyl benzoxazole/benzthiazole ligands were synthesized. Characterization of the synthesized complexes was performed by elemental analysis and various spectroscopic techniques like IR, UV-vis, NMR (1H , ^{13}C , ^{31}P) and ESI-mass spectrometry. The molecular structure of **1** and **2** was confirmed by single-crystal X-ray crystallography which revealed an octahedral geometry around ruthenium ion. Stability of the complexes in Tris-HCl/NaCl buffer was investigated using absorption spectroscopy which confirmed that they retain their molecular composition in the chosen buffer solution. Binding behavior of the new organoruthenium(II) complexes with DNA revealed the existence of intercalative mode of interaction. The binding ability of the new compounds is comparable to previously reported ruthenium complexes [70, 75, 76]. However, the new complexes are simple and their syntheses are relatively easy when compared to reported compounds. Moreover, **4** and **2** bind with DNA stronger than **3** and **1**, which could be a result of a deeper intercalation of the chromophore into the DNA due to the longer Ru-As (**4**, **2**) versus the Ru-P (**1**, **3**) bond distances. From the protein binding studies, the mechanism of quenching of BSA was found to be a static one, which indicates that the complexes bind to BSA via hydrophobic interaction. Apart from the above mentioned interaction with biomolecules, **1-4** exhibited promising catecholase-like activity for the oxidation of 3,5-DTBC to 3,5-DTBQ and phosphatase-like activity in the hydrolysis of 4-NPP to 4-NP.

Supplementary material

CCDC 1437107 (**1**) and 1437108 (**2**) contain the supplementary crystallographic data for this paper. These data can be obtained free of charge via <http://www.ccdc.cam.ac.uk/conts/retrieving.html>, or from the Cambridge Crystallographic Data Centre, 12 Union Road, Cambridge CB2 1EZ, UK; [Fax: +44-1223/150 336033; E-mail: deposit@ccdc.cam.ac.uk]. Representative NMR (1H , ^{13}C , ^{31}P) and ESI-MS spectra of the

complexes. Unit cell packing diagram for **1** and **2**. Fluorescence titrations of **1-3** (25 μM) with CT-DNA (0-50 μM). Fluorescence titrations of **1-3** (0-50 μM) with EB bound CT-DNA (7.5 μM). Fluorescence titrations of **1-3** (0-50 μM) with BSA (1 μM). Scatchard and Stern-Volmer plots of **1-4**. Oxidation of 3,5-DTBC by **2-4** monitored by fluorescence spectroscopy. Hydrolysis of 4-NPP by **2-4** monitored by fluorescence spectroscopy. Non-linear plots of catecholase and phosphatase activity of **1-4**.

Acknowledgement

One of the authors (A.G.) thanks the Department of Science and Technology, Ministry of Science and Technology, Government of India, for a fellowship under the INSPIRE scheme (No. IF140098). The authors also thank UGC, India for financial assistance to Department of Chemistry, Periyar University, Salem under SAP.

References

- [1] D.S. Sigman, T.W. Bruice, A. Mazumder, C.L. Sutton. *Acc. Chem. Res.*, **26**, 98 (1993).
- [2] J.K. Barton, A.M. Pyle. *Prog. Inorg. Chem.*, **38**, 413 (1990).
- [3] A.M. Burkhoff, T.D. Tullius. *Nature*, **331**, 455 (1988).
- [4] C.G. Riordan, P.J. Wei. *J. Am. Chem. Soc.*, **116**, 2189 (1992).
- [5] J.D. Tan, S.E. Hudson, S.J. Brown, M.M. Olmstead, P.K. Mascharak. *J. Am. Chem. Soc.*, **114**, 3841 (1992).
- [6] J.Q. Wang, Z.Z. Zhao, H.B. Bo, Q.Z. Chen. *J. Coord. Chem.*, **68**, 4408 (2015).
- [7] C.F. Chin, Q. Tian, M.I. Setyawati, W. Fang, E.S.Q. Tan, D.T. Leong, W.H. Ang. *J. Med. Chem.*, **55**, 7571 (2012).
- [8] X.L. Hong, W.G. Lu. *J. Coord. Chem.*, **69**, 177 (2016).
- [9] P. Heffeter, K. Bock, B. Atil, M.A. Reza Hoda, W. Körner, C. Bartel, U. Jungwirth, B.K. Keppler, M. Micksche, W. Berger, G. Koellensperger. *J. Biol. Inorg. Chem.*, **15**, 15737 (2010).
- [10] Z.H. Liang, Z.Z. Li, H.L. Huang, Y.J. Liu. *J. Coord. Chem.*, **64**, 3342 (2011).
- [11] C. Gossens, I. Tavernelli, U. Rothlisberger. *J. Am. Chem. Soc.*, **130**, 10921 (2008).
- [12] W. Guo, W. Zheng, Q. Luo, X. Li, Y. Zhao, S. Xiong, F. Wang. *Inorg. Chem.*, **52**, 3285 (2013).
- [13] C.G. Hartinger, M. Groessel, S.M. Meier, A. Casini, P.J. Dyson. *Chem. Soc. Rev.*, **42**, 6186 (2013).
- [14] Q.Q. Zhang, F. Zhang, W.G. Wang, X.L. Wang. *J. Inorg. Biochem.*, **100**, 1344 (2006).
- [15] F.A. French, E.J.J. Blanz. *Cancer Res.*, **25**, 1454 (1965).
- [16] X.W. Liu, J.S. Shu, Y. Xiao, Y.M. Shen, S.B. Zhang, J.L. Lu. *J. Coord. Chem.*, **68**, 2886 (2015).
- [17] R.H. Holm, P. Kennepohl, E.I. Solomon. *Chem. Rev.*, **96**, 2239 (1996).
- [18] U.K. Hansen. *Pharmacol. Rev.*, **33**, 17 (1981).
- [19] D.S. Raja, N.S.P. Bhuvanesh, K. Natarajan. *Inorg. Chem.*, **50**, 12852 (2011).
- [20] P. Vijayan, P. Viswanathamurthi, V. Silambarasan, D. Velmurugan, K. Velmurugan, R. Nandhakumar, R.J. Butcher, T. Silambarasan, R. Dhandapani. *J. Organomet. Chem.*, **768**, 163 (2014).
- [21] R. Manikandan, N. Chitrapriya, Y.J. Jang, P. Viswanathamurthi. *RSC Adv.*, **3**, 11647

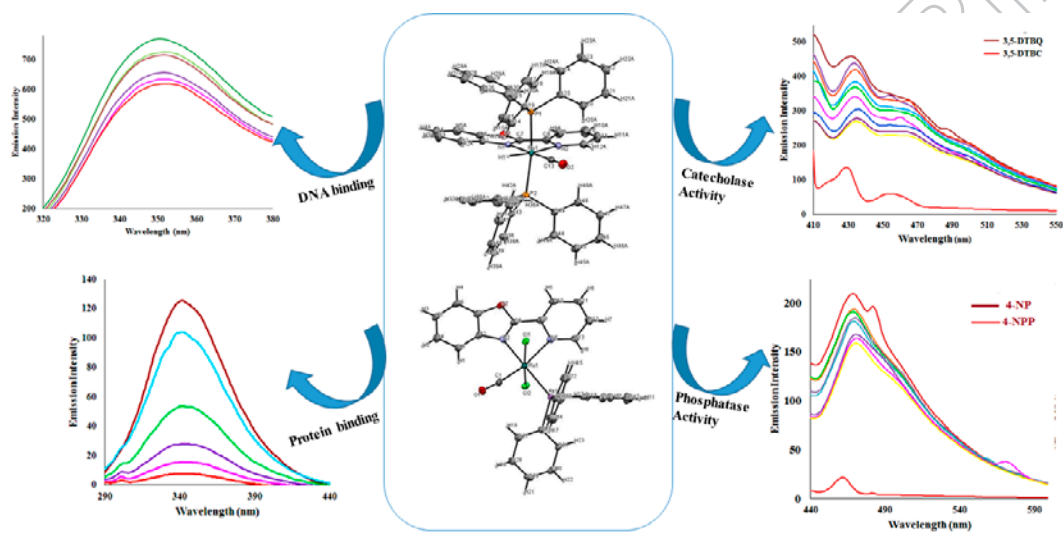
- (2013).
- [22] K. Zheng, F. Liu, X.M. Xu, Y.T. Li, Z.Y. Wu, C.W. Yan. *New J. Chem.*, **38**, 2964 (2014).
- [23] A.M. Traynor, J.W. Lee, G.K. Bayer, J.M. Tate, S.P. Thomas, M. Mazurczak, D.L. Graham, J.M. Kolesar, J.H. Schiller. *Invest. New Drugs*, **28**, 91 (2010).
- [24] P. Anitha, R. Manikandan, A. Endo, T. Hashimoto, P. Viswanathamurthi. *Spectrochim. Acta, Part A*, **99**, 174 (2012).
- [25] N.P.E. Barry, P.J. Sadler. *Chem. Commun.*, **49**, 5106 (2013).
- [26] A.C. Komor, J.K. Barton. *Chem. Commun.*, **49**, 3617 (2013).
- [27] C.G. Hartinger, N. Metzler-Nolte, P.J. Dyson. *Organometallics*, **31**, 5677 (2012).
- [28] G. Gassr, I. Ott, N. Metzler-Nolte. *J. Med. Chem.*, **54**, 3 (2011).
- [29] G.S. Smith, B. Therrien. *Dalton Trans.*, **40**, 10793 (2011).
- [30] A. Bergamo, S. Zorzet, B. Gava, A. Sorc, E. Alessio, E. Iengo, G. Sava. *Anticancer Drugs*, **11**, 665 (2000).
- [31] J.M. Rademaker-Lakhai, D. Van Den Bongard, D. Pluim, J.H. Beijnen, J.H.M. Schellens. *Clin. Cancer Res.*, **10**, 3717 (2004).
- [32] G. Sava, A. Bergamo, P.J. Dyson. *Dalton Trans.*, **40**, 9069 (2011).
- [33] K.J. Kilpin, P.J. Dyson. *Chem. Sci.*, **4**, 1410 (2013).
- [34] E. Meggers. *Angew. Chem. Int. Ed.*, **50**, 2442 (2011).
- [35] S. Aiello, G. Wells, E.L. Stone, H. Kadri, R. Bazzi, D.R. Bell, M.F.G. Stevens, C.S. Matthews, T.D. Bradshaw, A.D. Westwell. *J. Med. Chem.*, **51**, 5135 (2008).
- [36] J. Das, J. Lin, R.V. Moquin, Z. Shen, S.H. Spergel, J. Wityak, A.M. Doweiko, H.F. DeFex, Q. Fang, S. Pang, S. Pitt, D. Ren Shen, G.L. Schieven, J.C. Barrish. *Bioorg. Med. Chem. Lett.*, **13**, 2145 (2003).
- [37] A. Pinar, P. Yurdakul, I. Yildiz, O. Temiz-Arpaci, N.L. Acan, E. Aki-Sener, I. Yalcin. *Biochem. Biophys. Res. Commun.*, **317**, 670 (2004).
- [38] M.L. Perrone, E.L. Presti, S.D. Acqua, E. Monzani, L. Santagostini, L. Casella. *Eur. J. Inorg. Chem.*, 3493 (2015).
- [39] C. Gerdemann, C. Eicken, B. Krebs. *Acc. Chem. Res.*, **35**, 183 (2002).
- [40] A. Guha, T. Chattopadhyay, N.D. Paul, M. Mukherjee, S. Goswami, T.K. Mondal, E. Zangrando, D. Das. *Inorg. Chem.*, **51**, 8750 (2012).

- [41] I.A. Koval, P. Gamez, C. Belle, K. Selmeczi, J. Reedijk. *Chem. Soc. Rev.*, **35**, 814 (2006).
- [42] A. Hazari, L.K. Das, R.M. Kadam, A. Bauza, A. Frontera, A. Ghosh. *Dalton Trans.*, **44**, 3862 (2015).
- [43] Y.F. Chen, M. Liu, J.W. Mao, H.T. Song, H. Zhou, Z.Q. Pan. *J. Coord. Chem.*, **65**, 3413 (2012).
- [44] X. Zhang, X. Xu, H. Xu, X. Zhang, D.L. Phillips, C. Zhao. *ChemPhysChem*, **15**, 1887 (2014).
- [45] Y. Ning, M. Gao, K. Zheng, Z. Zhang, J. Zhou, X. Hao, R. Cao. *J. Mol. Catal. A*, **403**, 43 (2015).
- [46] S. Anbu, S. Kamalraj, B. Varghese, J. Muthumary, M. Kandaswamy. *Inorg. Chem.*, **51**, 5580 (2012).
- [47] E.Y. Tirel, Z. Bellamy, H. Adams, V. Lebrun, F. Duarte, N.H. Williams. *Angew. Chem. Int. Ed.*, **53**, 8246 (2014).
- [48] S. Anbu, M. Kandaswamy. *Inorg. Chim. Acta*, **385**, 45 (2012).
- [49] J. Gangopadhyay, S. Sengupta, S. Bhattacharyya, I. Chakraborty, A. Chakravorty. *Inorg. Chem.*, **41**, 2616 (2002).
- [50] G.M. Sheldrick, SHELXL97, *Program for Crystal Structure Refinement*, University of Gottingen, Germany (1997).
- [51] A. Altomare, G. Cascarano, C. Giacovazzo, A. Guagliardi, M. Burla, G. Polidori, M. Camalli. *J. Appl. Cryst.*, **27**, 435 (1994).
- [52] A. Bouchoucha, A. Terbouche, A. Bourouina, S. Djebbar. *Inorg. Chim. Acta*, **418**, 187 (2014).
- [53] B. Machura, R. Kruszynski, J. Kusz. *Polyhedron*, **27**, 1679 (2008).
- [54] E. Shuter, H.R. Hoveyda, V. Karunaratne, S.J. Rettig, C. Orvig. *Inorg. Chem.*, **35**, 368 (1996).
- [55] A. Ceulemans, L.G. Vanquickenborne. *J. Am. Chem. Soc.*, **103**, 2238 (1981).
- [56] L. Tan, J. Shen, J. Liu, L. Zeng, L. Jin, C. Weng. *Dalton Trans.*, **41**, 4575 (2012).
- [57] P. Anitha, N. Chitrapriya, Y.J. Jang, P. Viswanathamurthi. *J. Photochem. Photobiol., B*, **129**, 17 (2013).
- [58] J.G. Małecki. *Polyhedron*, **31**, 159 (2012).
- [59] E. Ramachandran, D. Senthil Raja, N.P. Rath, K. Natarajan. *Inorg. Chem.*, **52**, 1504

- (2013).
- [60] V. Mahalingam, N. Chitrapriya, F.R. Fronczek, K. Natarajan. *Polyhedron*, **29**, 3363 (2010).
- [61] S.B. Garber, J.S. Kingsbury, B.L. Gray, A.H. Hoveyda. *J. Am. Chem. Soc.*, **122**, 8168 (2000).
- [62] L. Delaude, A. Demonceau, A.F. Noels. *Chem. Commun.*, 986 (2001).
- [63] L. Delaude, M. Szypa, A. Demonceau, A.F. Noels. *Adv. Synth. Catal.*, **344**, 749 (2002).
- [64] A.A. Danopoulos, S. Winston, W.B. Motherwell. *Chem. Commun.*, 1376 (2002).
- [65] M. Poyatos, E. Mas-Marza, M. Sanau, E. Peris. *Inorg. Chem.*, **43**, 1793 (2004).
- [66] M. Baya, B. Eguillor, M.A. Esteruelas, M. Olivan, E. Onate. *Organometallics*, **26**, 6556 (2007).
- [67] M. Poyatos, W. McNamara, C. Incarvito, E. Clot, E. Peris, R.H. Crabtree. *Organometallics*, **27**, 2128 (2008).
- [68] W. Ghattas, H. Muller-Bunz, M. Albrecht. *Organometallics*, **29**, 6782 (2010).
- [69] Q. Yu, Y. Liu, J. Zhang, F. Yang, D. Sun, D. Liu, Y. Zhou, J. Liu. *Metallomics*, **5**, 222 (2013).
- [70] J.Q. Wang, Z.Z. Zhao, H.B. Bo, Q.Z. Chen. *J. Coord. Chem.*, **69**, 177 (2016).
- [71] P. Zhao, J. Li, L.J. Yang, J.Z. Lu, H.M. Guo, L.N. Ma, B.H. Ou. *J. Coord. Chem.*, **66**, 4220 (2013).
- [72] E. Jayanthi, M. Anusuya, N.S.P. Bhuvanesh, K.A. Khalil, N. Dharmaraj. *J. Coord. Chem.*, **68**, 3551 (2015).
- [73] J.Q. Wang, Z.Z. Zhao, H.B. Bo, Q.Z. Chen. *J. Coord. Chem.*, **69**, 177 (2016).
- [74] K.A. Kumar, K.L. Reddy, S. Satyanarayana. *J. Coord. Chem.*, **63**, 3676 (2010).
- [75] L. Xu, N.J. Zhong, Y.Y. Xie, H.L. Huang, Z.H. Liang, Z.Z. Li, Y.J. Liu. *J. Coord. Chem.*, **65**, 55 (2012).
- [76] J. Sun, W.X. Chen, X.D. Song, X.H. Zhao, A.Q. Ma, J.X. Chen. *J. Coord. Chem.*, **68**, 308 (2015).
- [77] C. Wang, Q. Wu, Y. Zeng, D. Huang, C. Yu, X. Wang, W. Mei. *J. Coord. Chem.*, **68**, 1489 (2015).
- [78] E. Ramachandran, P. Kalaivani, R. Prabhakaran, M. Zeller, J.H. Bartlett, P.O. Adero, T.R. Wagner, K. Natarajan. *Inorg. Chim. Acta*, **385**, 94 (2012).

- [79] C.B. Spillane, M.N.V. Dabo, N.C. Fletcher, J.L. Morgan, F.R. Keene, I. Haq, N.J. Buurma. *J. Inorg. Biochem.*, **102**, 673 (2008).
- [80] Q. Yu, Y. Liu, J. Zhang, F. Yang, D. Sun, D. Liu, Y. Zhou, J. Liu. *Metallomics*, **5**, 222 (2013).
- [81] F.J.M. Almes, D. Porschke. *Biochemistry*, **32**, 4246 (1993).
- [82] Y.J. Liu, Z.H. Liang, Z.Z. Li, J.H. Yao, H.L. Huang. *J. Organomet. Chem.*, **696**, 2728 (2011).
- [83] Y. Zhang, Z.D. Qi, D. Zheng, C.H. Li, Y. Liu. *Biol. Trace Elem. Res.*, **130**, 172 (2009).
- [84] H.H.Y. Liu, Z.H. Xu, X.H. Liu, P.X. Xi, Z.Z. Zeng. *Chem. Pharm. Bull.*, **57**, 1237 (2009).
- [85] P. Vijayan, P. Viswanathamurthi, K. Velmurugan, R. Nandhakumar, M.D. Balakumaran, P.T. Kalaichelvan, J.G. Malecki. *RSC Adv.*, **5**, 103321 (2015).
- [86] M. Das, R. Nasani, M. Saha, S.M. Mobin, S. Mukhopadhyay. *Dalton Trans.*, **44**, 2299 (2015).
- [87] J.P. Chyn, F.L. Urbach. *Inorg. Chim. Acta*, **189**, 157 (1991).
- [88] K. Du, J. Liang, Y. Wang, J. Kou, C. Qian, L. Ji, H. Chao. *Dalton Trans.*, **43**, 17303 (2014).

Graphical abstract



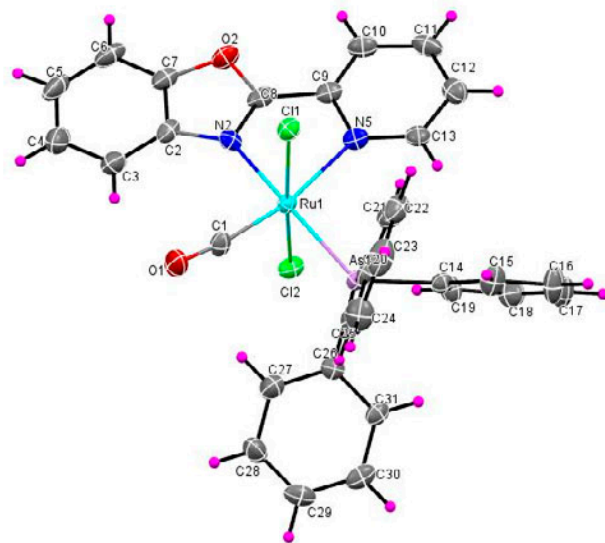


Figure 1. Perspective view (30% probability ellipsoids) of **2** with the atom numbering scheme.

ACCEPTED

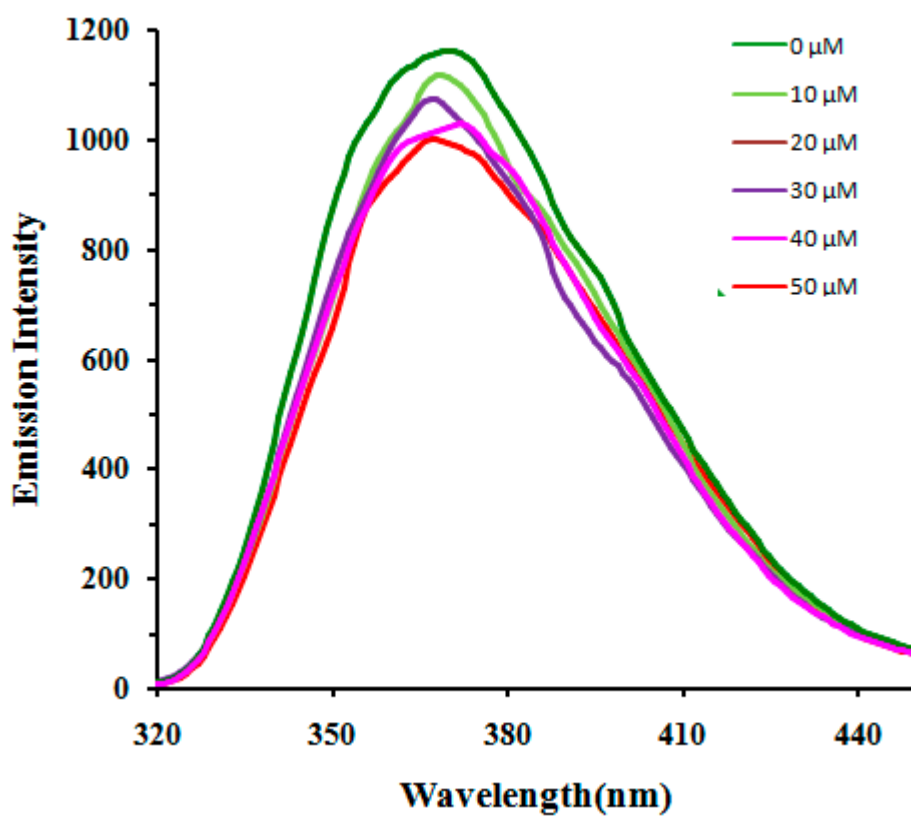


Figure 2. Fluorescence titrations of 4 (25 μM) with CT-DNA (0-50 μM).

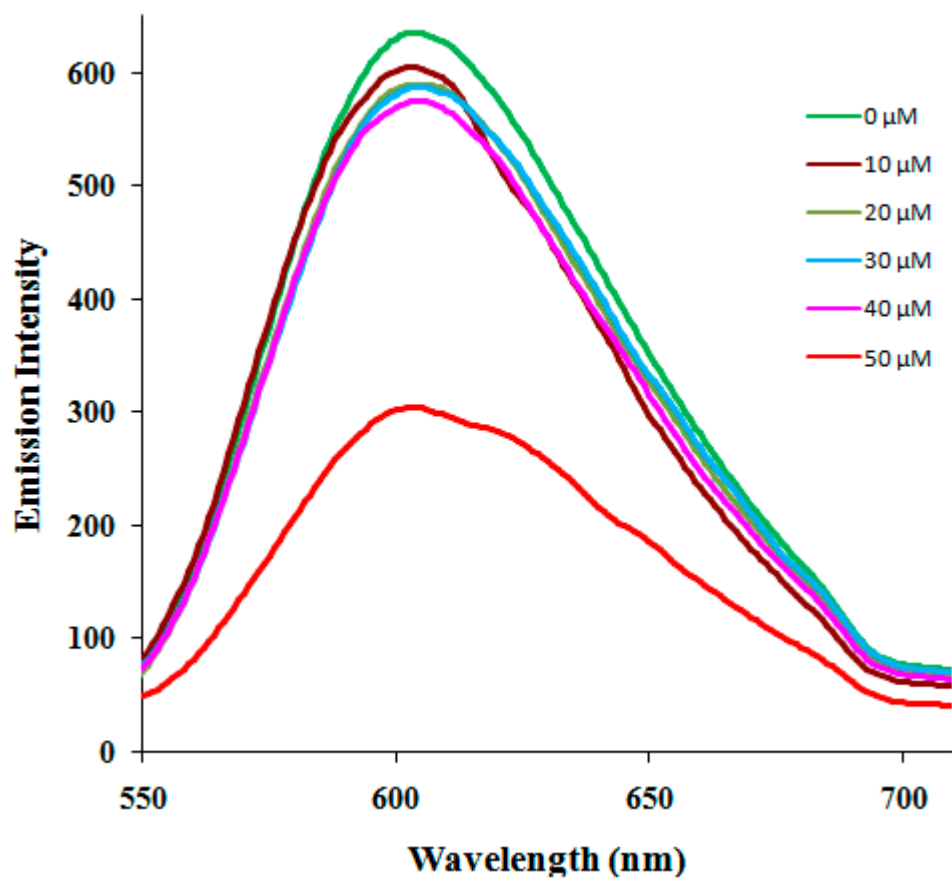


Figure 3. Fluorescence titrations of **4** (0-50 μM) with EB bound CT-DNA (7.5 μM).

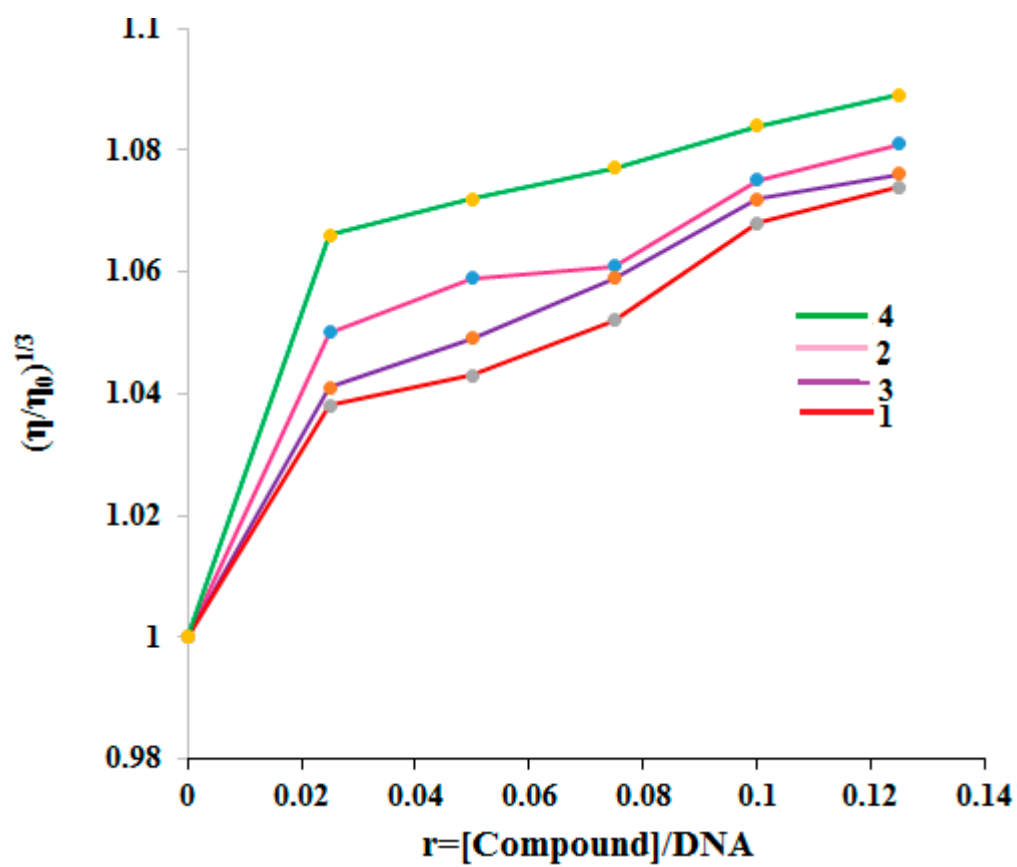


Figure 4. Relative viscosity $(\eta/\eta_0)^{1/3}$ of CT-DNA in Tris-HCl buffer solution in the presence of increasing amounts of **1-4** ($r = 0-0.1$).

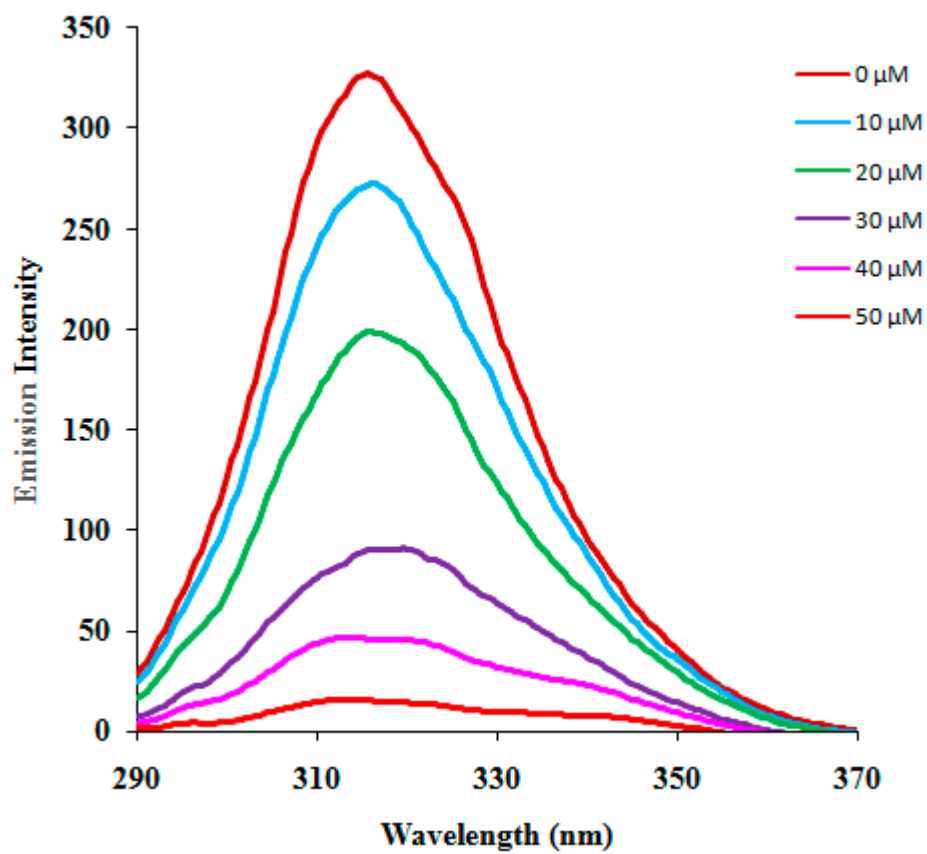


Figure 5. Fluorescence titrations of 4 (0-50 μM) with BSA (1 μM).

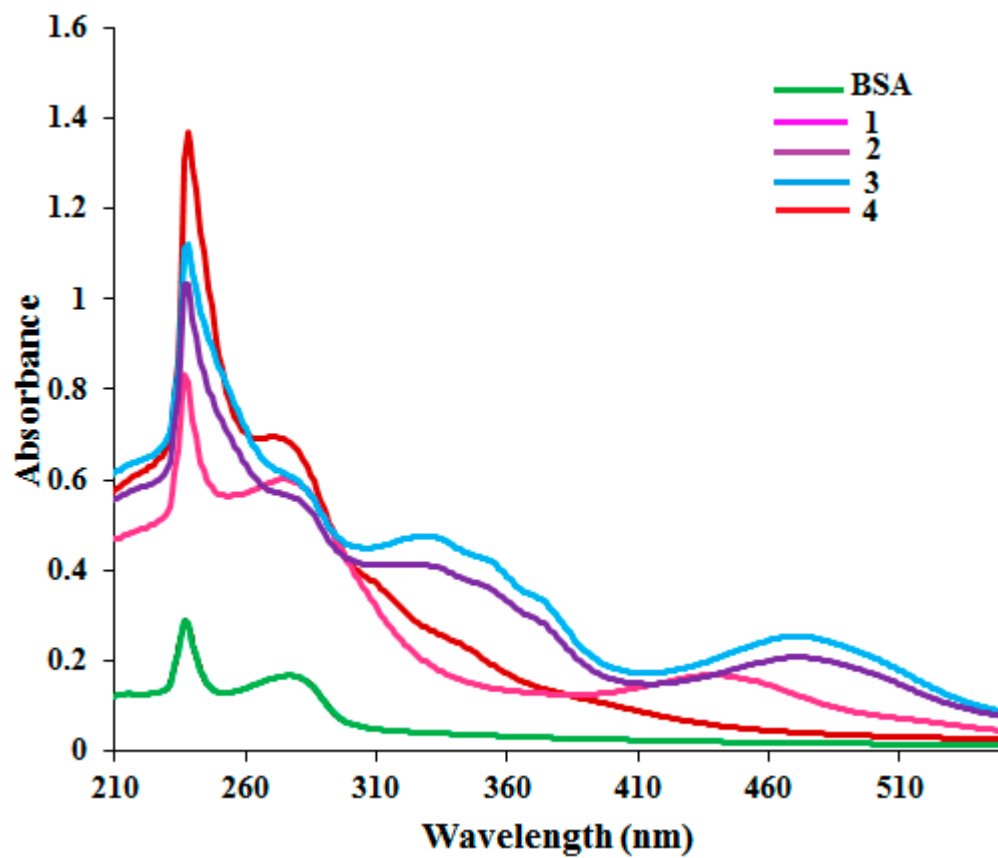


Figure 6. Absorbance spectra of 1-4 with BSA.

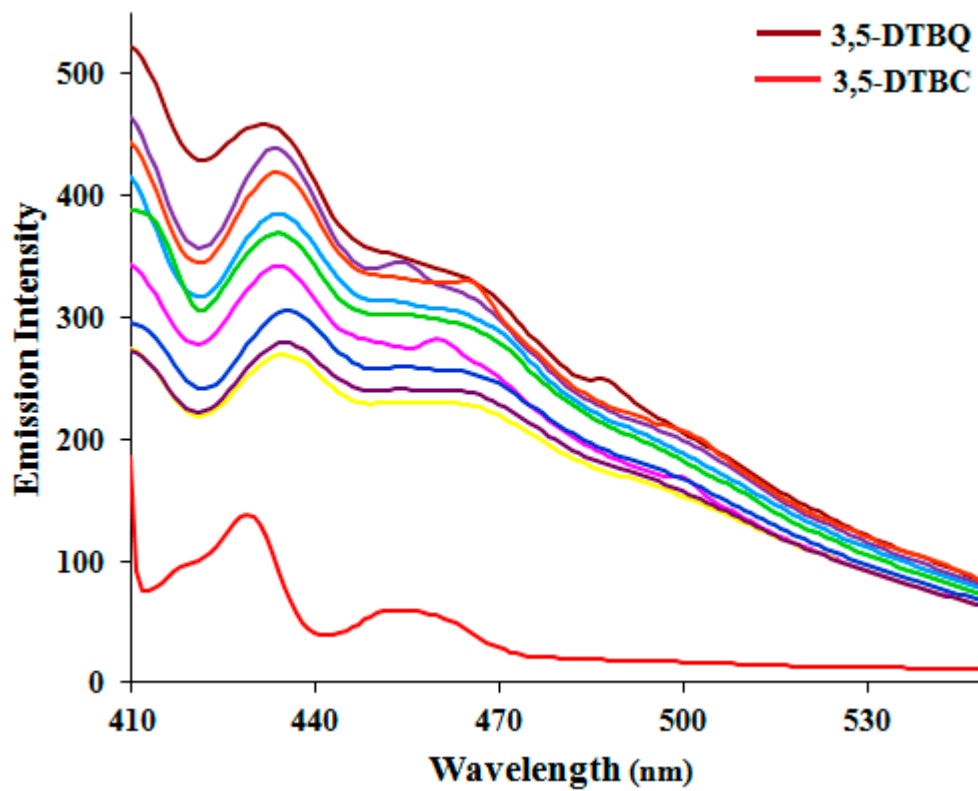


Figure 7. Oxidation of 3,5-DTBC by **1** monitored by fluorescence spectroscopy.

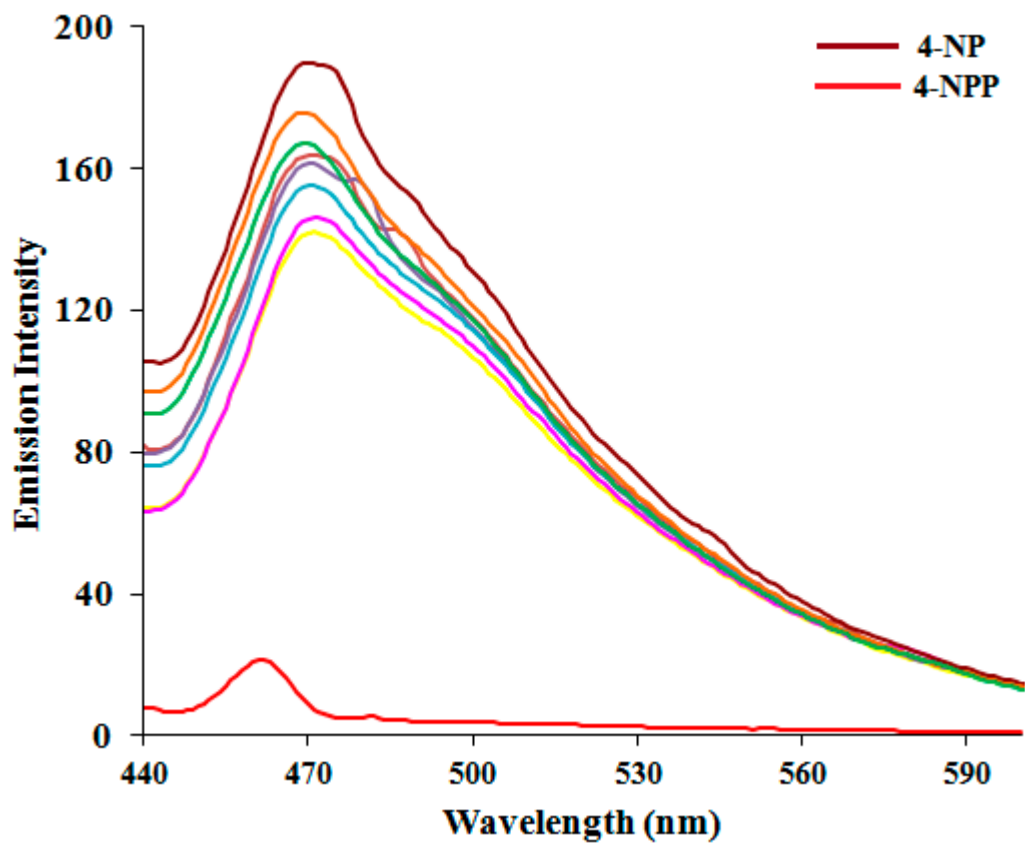


Figure 8. Hydrolysis of 4-NPP by **1** monitored by fluorescence spectroscopy.

Table 1. Crystal data and structure refinement for **2**.

| | |
|--|--|
| Empirical formula | C ₃₁ H ₂₃ AsCl ₂ N ₂ O ₂ Ru |
| Formula weight | 702.44 |
| Temperature (K) | 93.0(5) |
| Wavelength (Å) | 0.71075 |
| Crystal system | Triclinic |
| Space group | <i>P</i> -1 |
| Unit cell dimensions | |
| <i>a</i> (Å) | 9.307(10) |
| <i>b</i> (Å) | 9.673(10) |
| <i>c</i> (Å) | 15.847(16) |
| α (°) | 82.09(2) |
| β (°) | 89.70(3) |
| γ (°) | 86.23(2) |
| Volume (Å ³) | 1410(3) |
| <i>Z</i> | 2 |
| Density (calcd) Mg/m ⁻³ | 1.500 |
| Absorption coefficient (mm ⁻¹) | 1.942 |
| <i>F</i> (000) | 700.00 |
| Crystal size (mm ³) | 0.18 × 0.12 × 0.12 |
| Theta range for data collection (°) | 4.12 to 27.49 |
| Index ranges | -12 ≤ <i>h</i> ≤ 11 -12 ≤ <i>k</i> ≤ 11 -16 ≤ <i>l</i> ≤ 20 |
| Reflections collected | 10592 |
| Independent reflections | 6057 [R(int) = 0.0330] |
| Data / restraints / parameters | 6057 / 0 / 375 |
| Goodness-of-fit on <i>F</i> ² | 1.020 |
| Final R indices [<i>I</i> > 2σ(<i>I</i>)] | R1 = 0.0396, wR2 = 0.0942 |

Table 2. Selected bond lengths (Å) and angles (°) for **2**.

| Interatomic distances (Å) | |
|---------------------------|------------|
| Ru(1)-N(2) | 2.120(4) |
| Ru(1)-N(5) | 2.234(3) |
| Ru(1)-Cl(1) | 2.3974(19) |
| Ru(1)-Cl(2) | 2.397(2) |
| Ru(1)-C(1) | 1.829(4) |
| Ru(1)-As(1) | 2.4630(18) |
| | |
| As(1)-Ru(1)-Cl(1) | 95.45(7) |
| As(1)-Ru(1)-Cl(2) | 88.33(7) |
| As(1)-Ru(1)-N(2) | 175.15(8) |
| As(1)-Ru(1)-N(5) | 101.81(10) |
| As(1)-Ru(1)-C(1) | 88.21(13) |
| Cl(1)-Ru(1)-N(2) | 172.34(3) |
| Cl(1)-Ru(1)-N(5) | 88.73(11) |
| Cl(1)-Ru(1)-C(1) | 90.68(13) |
| Cl(2)-Ru(1)-N(2) | 87.23(10) |
| Cl(2)-Ru(1)-N(5) | 88.86(10) |
| Cl(2)-Ru(1)-C(1) | 96.11(13) |
| N(2)-Ru(1)-N(5) | 76.13(12) |
| N(2)-Ru(1)-C(1) | 94.23(15) |
| N(5)-Ru(1)-C(1) | 168.98(14) |
| Ru(1)-As(1)-C(14) | 115.45(11) |
| Ru(1)-As(1)-C(20) | 117.30(12) |
| Ru(1)-As(1)-C(26) | 116.17(12) |
| Ru(1)-N(2)-C(2) | 139.60(3) |
| Ru(1)-N(2)-C(8) | 114.70(3) |
| Ru(1)-N(5)-C(9) | 113.80(3) |
| Ru(1)-N(5)-C(13) | 129.40(3) |
| Ru(1)-C(1)-O(1) | 173.10(4) |

Table 3. Fluorescence spectral parameters for **1-4** binding with CT-DNA.

| Complex | K_{bin} | K_{sv} | K_{app} |
|----------|-----------------------------|--------------------|--------------------|
| 1 | $4.16 \times 10^4 \pm 0.03$ | 1.10×10^4 | 4.96×10^5 |
| 2 | $4.83 \times 10^4 \pm 0.04$ | 1.51×10^4 | 6.81×10^5 |
| 3 | $4.50 \times 10^4 \pm 0.02$ | 1.20×10^4 | 6.25×10^5 |
| 4 | $4.99 \times 10^4 \pm 0.05$ | 8.20×10^5 | 9.37×10^5 |

Table 4. Quenching parameters of BSA for **1-4**.

| Complex | K_q | K_{sv} | K_{bin} | 'n' |
|----------|---------------------|------------------------|----------------------------|------|
| 1 | 1.145×10^5 | 1.145×10^{13} | $1.7 \times 10^5 \pm 0.04$ | 1.08 |
| 2 | 1.563×10^5 | 1.563×10^{13} | $8.0 \times 10^6 \pm 0.06$ | 1.31 |
| 3 | 1.239×10^5 | 1.239×10^{13} | $1.9 \times 10^5 \pm 0.01$ | 1.43 |
| 4 | 2.325×10^5 | 2.325×10^{13} | $1.0 \times 10^7 \pm 0.02$ | 1.82 |

Table 5. Kinetic parameters for the catecholase activity of **1-4**.

| Catalyst | $K_M (M)$ | $V_{max}(Mm^{-1})$ | $k_{cat}(h^{-1})$ |
|----------|-----------------------|-----------------------|-------------------|
| 1 | 1.35×10^{-5} | 20.0×10^{-3} | 1350 |
| 2 | 2.27×10^{-4} | 7.90×10^{-4} | 227.8 |
| 3 | 1.33×10^{-5} | 1.11×10^{-3} | 1335 |
| 4 | 2.26×10^{-4} | 2.71×10^{-5} | 226.5 |

Table 6. Kinetic parameters for the phosphatase activity of **1-4**.

| Catalyst | $K_M(M)$ | $V_{max}(Mm^{-1})$ | $k_{cat}(h^{-1})$ |
|----------|-----------------------|-----------------------|-------------------|
| 1 | 1.02×10^{-3} | 1.79×10^{-3} | 204×10^1 |
| 2 | 6.63×10^{-3} | 2.93×10^{-3} | 132×10^1 |
| 3 | 6.43×10^{-2} | 3.16×10^{-3} | 176×10^1 |
| 4 | 8.84×10^{-2} | 8.40×10^{-4} | 128×10^1 |